IEEE Photonics Journal
An IEEE Photonics Society Publication

Open Access

A Numerical Model for Studying Multimicrochip and Single-Chip LEDs With an Interdigitated Mesa Geometry

Volume 5, Number 2, April 2013

Farn-Shiun Hwu
Ti-Hsiang Sung
Chun-Hung Chen
Jia-Wei Tseng
Heng Qiu
Jyh-Chen Chen

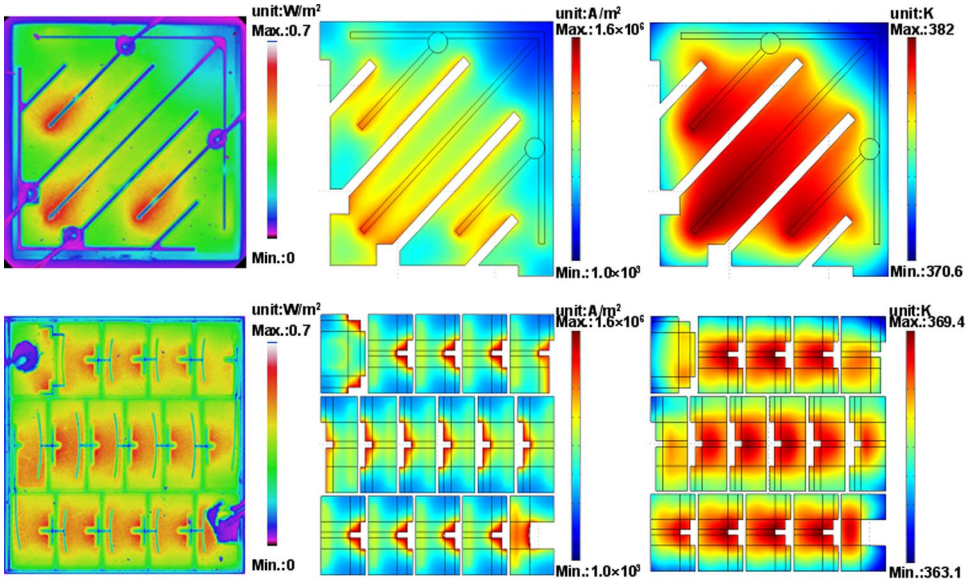

DOI: 10.1109/JPHOT.2013.2250275
1943-0655/$31.00 ©2013 IEEE

IEEE photonics SOCIETY

IEEE

A Numerical Model for Studying Multimicrochip and Single-Chip LEDs With an Interdigitated Mesa Geometry

Farn-Shiun Hwu,[1] Ti-Hsiang Sung,[2] Chun-Hung Chen,[2] Jia-Wei Tseng,[2] Heng Qiu,[2] and Jyh-Chen Chen[2]

[1]Department of Mechanical Engineering, Taoyuan Innovation Institute of Technology, Jhongli City 32091, Taiwan
[2]Department of Mechanical Engineering, National Central University, Jhongli City 32001, Taiwan

DOI: 10.1109/JPHOT.2013.2250275

Manuscript received January 31, 2013; revised February 23, 2013; accepted February 25, 2013. Date of publication March 7, 2013; date of current version March 12, 2013. This work was supported by the National Science Council of Taiwan through Grants NSC 101-2221-E-253-006 and NSC 101-2221-E-008-033-MY3. Corresponding author: J.-C. Chen (e-mail: jcchen@cc.ncu.edu.tw).

Abstract: A 3-D numerical model has been developed to investigate the transient thermal, electrical, and optical output performance of a single-chip light-emitting diode (LED) with an interdigitated mesa geometry under dc operation and a multimicrochip LED under either dc or full-wave operation. These two LED chips are fabricated on the same sapphire wafer. The junction temperature, the light output power, and the electroluminescence intensity of both LEDs are measured under dc to prove the results of the numerical simulations. The numerical simulation results are in good agreement with the experimental ones. The numerical results indicate that the multimicrochip LED under dc operation will demonstrate the best thermal and light output performance. Utilizing the input power considered in the present computation, the light output power for the multimicrochip LED, under either dc or full-wave operation, is raised continuously. On the other hand, the saturation of the light output is observed for the single-chip LED with interdigitated mesa geometry.

Index Terms: Full-wave, high-voltage light-emitting diodes (HV LED), junction temperature, multimicrochip.

1. Introduction

The progress made in the development of solid-state lighting technology over the last decade has increased its applications in light-emitting diodes (LEDs). The many advantages of LEDs, such as their narrow spectrum, long lifetime, and good mechanical stability [1], have led to them gradually replacing some conventional light sources. High-brightness LEDs have demonstrated excellent ability to function in back and general lighting applications [2]. In addition, the superior heat dissipation and better current spreading of the LED make it able to operate under higher power conditions. There are some methods to increase the light output of a LED chip, e.g., to design a better electrode pattern for a single LED chip [1], [3]–[6] and to manufacture a monolithic LED chip array [7], [8]. When the input power of a LED chip is enlarged, it results in an increase in the current and heat crowding. Therefore, some methods have been developed to improve the current spreading and heat transfer in LED chips by means of the optimum design of the electrode pattern and the geometry of the epitaxial structure [3]–[6]. Chakraborty *et al.* [7] fabricated an interdigitated multipixel array (IMPA) chip, which can suppress the current crowding and thereby improve the LED performance at high current injection. The chip array employed in the LED can increase the energy

utilization efficiency and reliability [9]. The current distribution in the LED chip is affected by the size and pattern of the electrode, as well as the material properties of the chip [5], [10]–[12] and cannot be measured directly but is usually estimated from the light output. A better design for the electrode pattern in monolithically integrated LED arrays can also increase the light emitting ratio and decrease the thermal burden [8]. This device will have excellent performance even when operating at high power. The efficiency droop in nitride-based LEDs [3], [13]–[15] still presents an important limitation for achieving high-power and low-cost emitters. Besides, the recent progress in the development of InGaN-based LEDs also includes enhancement of their internal quantum efficiency [16]–[18], improvement of material quality [19]–[21], and novel methods to achieve improved light extraction from resultant devices [22]–[24]. In addition, the potential of using integrated III-Nitride alloy as monolithic thermoelectric devices for achieving active solid state cooling in high-power LEDs has been examined in recent work [25]–[27].

Many different structures of LED chips have been designed and fabricated in the search for superior LED performance [1], [5], [7], [28]. However, this procedure is expensive and time consuming. To save expense and time, the use of analytical models has been proposed to explain the current spreading phenomenon and then to design a better device structure of LEDs [29], [30]. A 2-D numerical model was developed by Guo *et al.* [31] that incorporated the interdigitated mesh pattern into the LED to obtain a more uniform current spreading. Hwang *et al.* [32] developed a 3-D numerical simulation model incorporating the concept of series and parallel connections to investigate the current spreading in a LED. Recently, the finite-element scheme has been utilized to compute the electric potential and current density distribution in the LED chip directly, through the continuity equation of electronic transport [6], [33]. With this approach, the simulation of complex LED structures becomes possible.

The influence of the thermal effect on the performance of the LED has been considered in numerous studies [5], [10], [11], [28], [29], [32]. Kim *et al.* [5] showed in their experiments that, in the case of a small electrode, the output power saturation may occur for higher input power, and they have conjectured that the degradation of output power may be due to the enhancement of device resistance from the thermal effect. A higher temperature in the LED will reduce the voltage drop across the contact and the junction [28] and degrade the lifetime of the LED device [29], [34]. The heat causes a decline in the luminous efficacy [10], [11], [32] and a change in the color rendering index, with a shift of the point of chromaticity toward the blue end of the spectrum, raising the color temperature [34], [35]. Heat from nonradiative recombination and Joule heating are the two main sources of the thermal effect in LED chips [11], [28], [29], [32]. The nonradiative recombination in the active region is the dominant source of heat at lower current conditions. However, the Joule heating becomes significantly more important at higher current conditions since the Joule heating is proportional to the square of current [36]. However, the size of the LED chip is so tiny that the temperature distribution and the local current density in each layer are difficult to measure. At the present time, the junction temperature of LEDs is commonly measured by the forward-voltage method [36]–[39]. Bogdanov *et al.* proposed a numerical model based on the finite volume method, which was used to simulate an IMPA LED and a conventional lateral injection LED [40], [41]. The IMPA LED was designed with the parallel connection idea to avoid the problem of current crowding and overheating in the active region. They compared the numerical results with the experimental results obtained by Chakraborty *et al.* [7] and obtained a good agreement in the output optical power but had some errors in current–voltage (I–V) characteristics. Hwu *et al.* [42] extended the numerical model proposed by Chen and his coworkers [6], [33] to include the thermal effect. A simulation was performed for vertical LED chips with different n-electrode areas taking into account the effect of current blocking layer size. The results are in good agreement with the experimental ones obtained by Kim *et al.* [5]. Tu *et al.* [1] fabricated high-power ThinGaN LED chips with different electrode patterns and employed the numerical simulation tool developed by [6], [33] to investigate the electrical characteristics of these samples. At the present time, there is no numerical model able to simulate a transient problem or account for the saturation effect of light output.

Nowadays, LEDs driven by alternating current (ac) are receiving much attention due to their characteristics of high voltage (HV) and low current [38], [39], [43], [44]. They are also convenient to

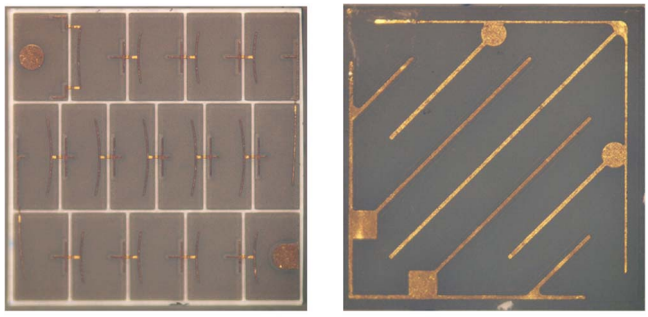

(a) (b)

Fig. 1. (a) Multimicrochip LED and (b) single-chip LED with the interdigitated mesa geometry.

operate in an ac utility system. In contrast, the traditional dc LED chip can be powered by a few volts of direct current, but a transformer and a rectifier are needed for operation in the utility system. A novel LED chip array, usually known as a HV LED, can be driven by either an ac or a dc source through a full-wave rectifier [45]. Under ac source operation, all microchips for the HV LED are simultaneously turned on according to the ac cyclic when the threshold voltage is reached. This can improve the drawback of an ac LED where only part of the radiation area is turned on in each bias direction. However, the transient characteristics of the temperature, electrical, and light output of HV LEDs are difficult to observe under ac operation. Therefore, it is necessary to develop a proper unsteady numerical model to understand these characteristics.

In this paper, the numerical model developed in our previous work [6], [33], [42] has been modified and expanded to be capable of accounting for the transient behavior and the saturation effect of the light output power. A numerical simulation has been performed to investigate the thermal, electrical, and light output performances of the HV LED and the single-chip LED with an interdigitated mesa structure under different input powers. To verify the numerical results, the junction temperature, the light output power, and the electroluminescence (EL) intensity are measured under dc operation. Besides, the transient behavior of the HV LED under the full-wave operation is predicted through a series of numerical simulation.

2. Simulation and Experiment

2.1. Numerical Model

An HV LED chip with 16 series-connected microchips and a single-chip LED with an interdigitated mesa geometry are analyzed, as shown in Fig. 1(a) and (b), respectively. The full chip dimensions are 1.2 mm $\times$ 1.2 mm $\times$ 106 μm in both cases. Each microchip in the top and bottom rows is 0.22 mm $\times$ 0.35 mm, while those in the middle row are 0.18 mm $\times$ 0.43 mm. Photographs were taken using a digital camera (E-420, Olympus) with the ISO value set to 200 through an optical microscope (BX60, Olympus). In order to ensure that the two LED chips have the same material properties and epitaxial structure, the GaN LED chips are fabricated on the same wafer. They are mounted on a copper lead frame with an aluminum heat-dissipating fin (39 mm $\times$ 37 mm $\times$ 17 mm), as shown in Fig. 2. A schematic representation of a cross section in the lateral direction of the LED chips is shown in Fig. 3. The thicknesses of the ITO layer, *p*-type GaN layer, active layer, *n*-type GaN layer, and sapphire are 0.5, 0.2, 0.8, 4.5, and 100 μm, respectively.

The continuity equation for electronic transport in a LED chip is

$$\frac{[\nabla\partial \cdot \varepsilon(\nabla \cdot V)]}{\partial t} + \nabla \cdot (\sigma \nabla V) = 0 \tag{1}$$

where ε is the relative dielectric constant (8.9 for GaN) [36], t is the time, σ is the conductivity, and V is the electrical potential. The resistivities $(\rho = 1/\sigma)$ of the electrodes, ITO, *p*-GaN, and *n*-GaN are

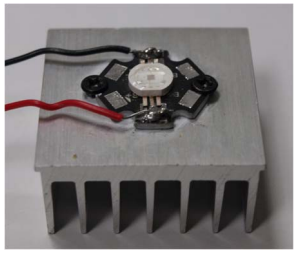

Fig. 2. LED packaged with an aluminum heat-dissipating fin.

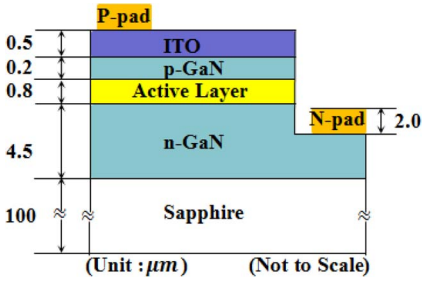

Fig. 3. Cross-sectional schematic representation of the LED chips in the lateral direction.

$7.25 \times 10^{-6}\ \Omega \cdot \text{cm}$, $1 \times 10^{-3}\ \Omega \cdot \text{cm}$, $14\ \Omega \cdot \text{cm}$, and $1 \times 10^{-2}\ \Omega \cdot \text{cm}$, respectively. Following our previous work [42], the current through the active layer is assumed to be in the direction perpendicular to the layer. Otherwise, the specific *p*- and *n*-contact resistances are also following our previous work [42]. The equation for calculating the electrical potential in the LED is solved using the finite-element method (FEM). The equivalent conductivity for each element in the active layer is proposed by

$$\sigma = \frac{l_e}{V_j} \cdot J_e \tag{2}$$

where l_e is the elemental thickness of the mesh, V_j is the voltage drop between the active layer, and J_e is the elemental current density. The current behavior through the active layer of the LED chip is dominated by the Shockley equation

$$J_e = J_0\left(\exp^{\frac{eV_j}{nkT}} - 1\right) \tag{3}$$

where J_0 is the saturation current density, e is the elementary charge $(1.6 \times 10^{-19}\ \text{coul})$, n is the ideality factor, k is the Boltzmann constant $(1.38 \times 10^{-23}\ \text{J/K})$, and T is the absolute temperature. It is well known that J_0 and n are dependent on the material quality and/or device structure. Therefore, the values of J_0 and n are calculated using our measurement of the *I*–*V* characteristics. The *p*-pad is set to have a uniform input current, and the *n*-pad is set as the ground. With the exception of the electrodes, the rest of the boundaries in the LED chip are all assumed to be insulated.

The equation of conduction heat transfer with the heat source is

$$DC_p \frac{\partial T}{\partial t} - \nabla \cdot (k_c \nabla T) = \dot{q} \tag{4}$$

where D is the density, C_p is the specific heat, and k_c is the thermal conductivity. Based on the law of energy conservation, the input electrical power is transferred into two major parts: one is the light

TABLE 1
Thermal conductivities of the LED materials

Material	Al	Cu	Au	ITO	sapphire	GaN
k_c (W/m · K)	204	386	290	10	35	130

output power (P_{out}), and the other is the heat generation. The ratio of the light output power to the input electrical power in the active layer is known as the conversion efficiency [46],

$$\eta_{\text{CE}} = \frac{P_{\text{out}}}{IV_j} \tag{5}$$

where I is the current. The η_{CE} used in our numerical simulation are determined from the experiment by measuring the P_{out} and I. And the V_j is calculated by deducting the product of current and series resistance [10] of LED from the forward voltage obtained by the measurement of the I–V characteristics. Thus, we propose the heat generation term $\dot{q}$ in the active layer as follows:

$$\dot{q} = \frac{J_e V_j}{l_e}(1 - \eta_{CE}). \tag{6}$$

The heat generation term per unit volume $\dot{q}$ due to Joule heating in the layers of the LED chip except the active one is

$$\dot{q} = J_e \cdot \nabla V. \tag{7}$$

The heat from the absorption of light output power in LED chip is considered in the term of active layer. The thermal conductivities of the materials inside the LED are summarized in Table 1 [40], [46]–[48].

The thermal boundary condition at the surface of the LED packaged with an aluminum heat-dissipating fin (see Fig. 2) is assumed to be

$$\hat{n} \cdot (k_c \nabla T) = h(T_{\text{inf}} - T) \tag{8}$$

where $\hat{n}$ is the unit normal vector of the interface, T_{inf} is the air temperature, and h is the convective heat transfer coefficient. Here, we select $h = 5$ W/m^2 · K and $T_{\text{inf}} = 290$ K since the LED is under the natural convection environment.

The thermal and electrical equations mentioned above are solved with the FEM method to obtain the temperature, the electrical potential, and the current density in the LED chip. The mesh for each layer is made up of pentahedron elements. Convergence testing of a LED chip with an interdigitated mesa structure has been performed for element numbers of the entire packaging with 120483, 152104, 351189, and 459695. The simulation results for temperature, current density, and voltage are almost the same as for the cases of 351189 and 459695. To save on computational memory and the computation time, the number of finite elements is chosen to be 351189 for the entire packaging domain, and the relative tolerance is selected to be 1×10^{-3} for the variables of temperature and voltage. Fig. 4 shows the element structure for the LED chip with an interdigitated mesa structure and the heat-dissipating fin. Convergence testing is also carried out for the case of the HV LED, with the number of finite elements chosen to be 344026.

2.2. Experimental Setup for Measuring the Junction Temperature

A system based on the forward-voltage method [36], [39] has been constructed to measure the junction temperature of the present LEDs, as shown in Fig. 5. This system consists of a temperature-controlled oven (BC-02, Poworld), a source meter (2400, Keithley), a computer, a temperature sensor with a T-type thermocouple, and a sample testing room (EIA/JESD 51-2 Industrial Standards). For calibration measurement, the LED is placed in a temperature-controlled

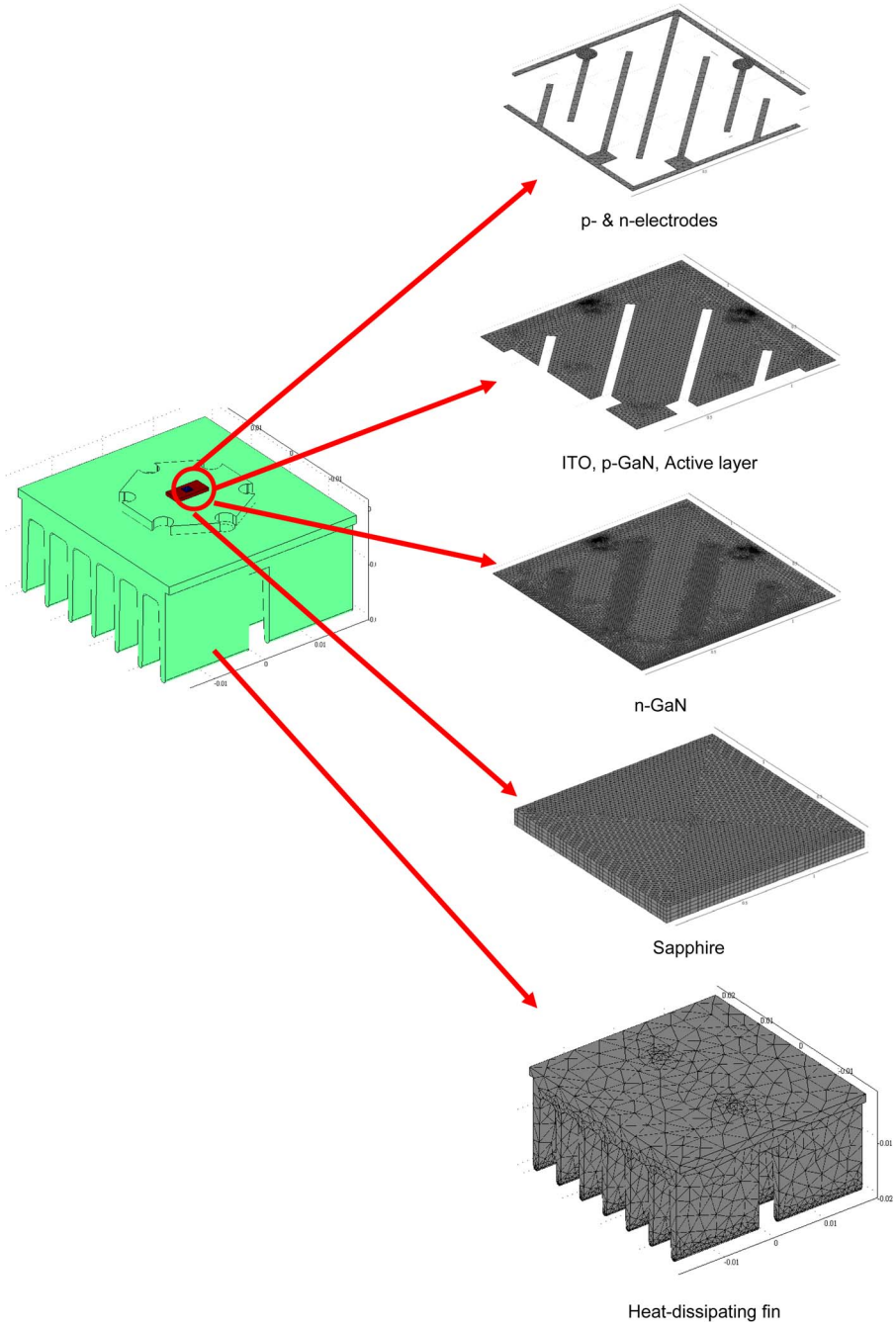

Fig. 4. Pentahedron element structure of each layer in the LED chip with an interdigitated mesa structure.

oven. The calibration is executed in a pulsed low current mode to avoid heat generation in the LED. The forward voltages are measured at different oven temperatures. During the calibration process, the linear relationship between the forward voltage and the junction temperature is obtained. This relationship provides a constant slope, called the K-factor. Subsequently, the LED is placed in the sample test room and driven by a working current. The forward voltage is measured when thermal equilibrium is reached. The forward voltage is again measured after switching to the low current. The difference in forward voltages between the working current and the low current is divided by the

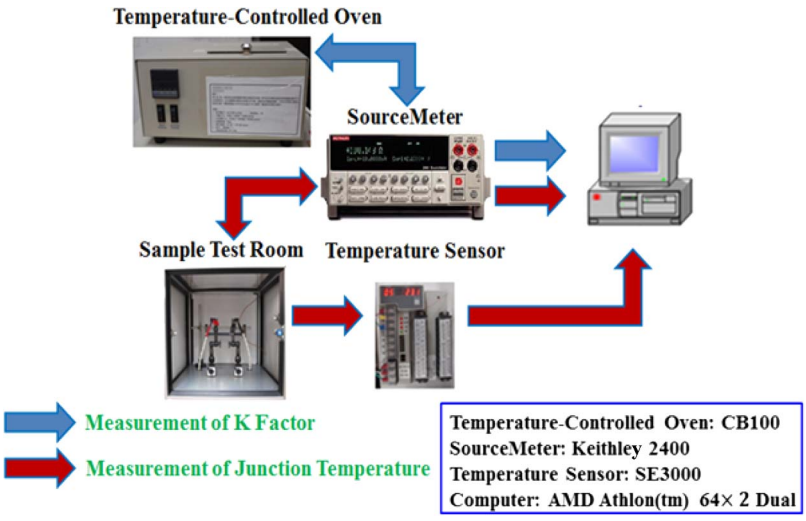

Fig. 5. System for measuring the junction temperature of an LED.

TABLE 2

Values of J_0 and n for the LED chips

Type of LED chip	J_0 (A/m^2)	n
Multi-microchip	3.61×10^{-16}	2.25
Single chip	3.88×10^{-24}	1.54

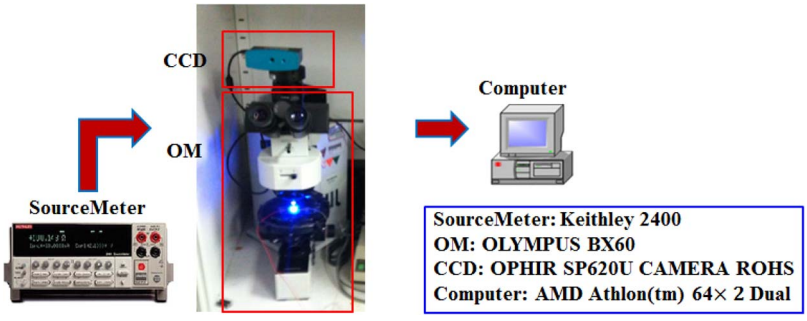

Fig. 6. System for measuring the EL intensity of an LED.

K-factor to obtain the temperature difference. The junction temperature is equal to the temperature difference plus the ambient temperature. Otherwise, the values of J_0 and n are determined from the I–V characteristics of the two types of LED under dc operation and are shown in Table 2.

2.3. Experimental Setup for Measuring the EL Intensity and Light Output Power

The system for measuring the EL intensity of the LED is comprised of an optical microscope (BX60, Olympus) and a camera (SP620U, Ophir) with a charge coupled device (CCD; Fig. 6). The EL intensity is transferred into the digital signal and is then shown on the computer monitor. An integrating sphere (12.5 in, Sphere Optics) and a spectroscope (USB2000, Ocean Optics) are set up to measure the light output power from the LED (see Fig. 7).

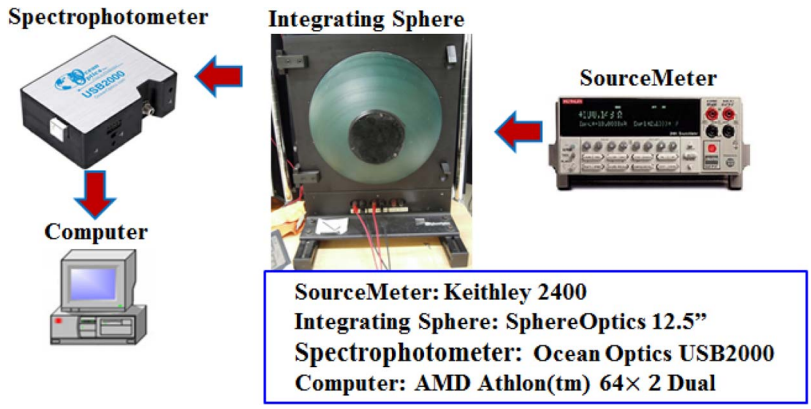

Fig. 7. System for measuring the light output power of an LED.

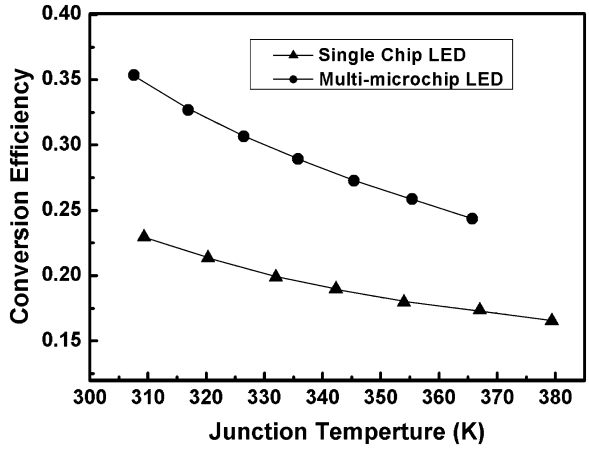

Fig. 8. Correlations between the conversion efficiency and junction temperature for the multimicrochip and single-chip setups.

3. Results and Discussion

Fig. 8 shows the conversion efficiencies (η_{CE}) for different junction temperatures (T_j) determined from the experimental measurements under dc operation. The correlations between the η_{CE} and T_j for the multimicrochip and single-chip setups are $\eta_{CE} = 46.656 \times \exp(-T_j/54.395) + 0.190$ and $\eta_{CE} = 5.104 \times \exp(-T_j/81.386) + 0.116$, respectively. The junction temperature for the single-chip LED under 4-W input power is about 380 K. To protect the LED sample, the experiment is not carried out for the power higher than 4 W.

Figs. 9 and 10 show the EL intensity at the chip surface and the simulated current density and temperature distributions at the active layer for the two LED chips for a 4-W input power under dc operation. For the single-chip LED, the current crowding appears in the region near the apex of the *p* electrode. On the other hand, the current crowding for the multimicrochip LED occurs in the region near the *n* electrode. The EL intensity and the temperature are higher in these regions. The difference between the higher and lower current densities for the multimicrochip LED is higher than that for the type with a single chip, but the current distribution in the multimicrochip LED is more uniform than that in the single-chip LED with an interdigitated mesa geometry. Therefore, the EL distribution of the multimicrochip LED is also more uniform than that of single-chip one. The maximum junction temperatures for the single chip and the multimicrochip are 382 K and 369.4 K, respectively. The differences between the maximum and minimum junction temperatures of the

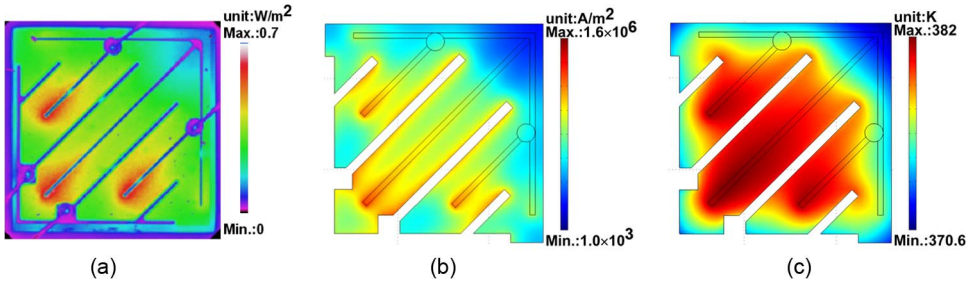

Fig. 9. Distribution of (a) EL intensity at the chip surface (measured), (b) current density (simulated), and (c) temperature (simulated) at the active layer of the single-chip LED.

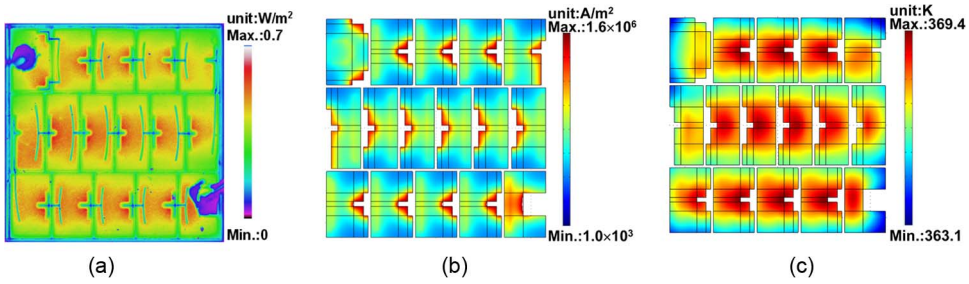

Fig. 10. Distribution of (a) EL intensity at the chip surface (measured), (b) current density (simulated), and (c) temperature (simulated) at the active layer of the multimicrochip LED.

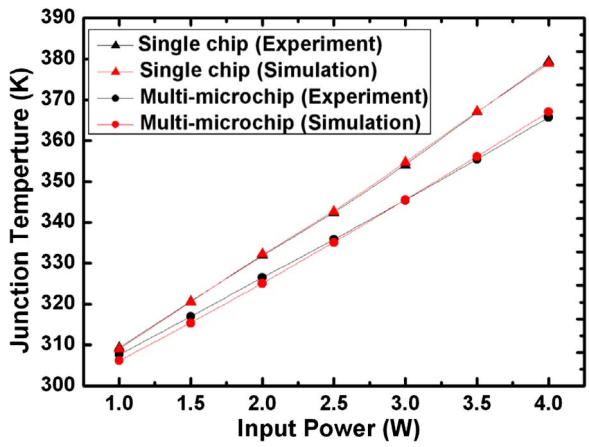

Fig. 11. Simulated and experimental junction temperatures of the two LED chips for different input powers.

single-chip LED and the multimicrochip LED are 11.4 K and 6.3 K, respectively. The lower junction temperature difference for the multimicrochip LED can be expected since the current density distribution is more uniform than that of the single-chip LED.

The average junction temperatures under different input powers for the two different LED chips obtained from the numerical simulation are compared with the experimental temperatures, as shown in Fig. 11. The numerical results are in good agreement with the experimental ones. The junction temperature increases almost linearly as the input power increases. The difference of the junction temperature between two LED chips is more significant for higher temperatures. The conversion efficiency decreases as the junction temperature becomes higher. Hence, the experimental

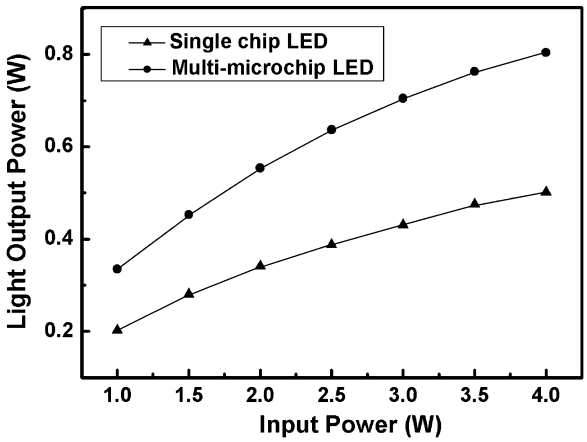

Fig. 12. Light output power versus the input power of the two LED chips by experimental measurements.

light output power difference between two LED chips increases when the input power is higher (see Fig. 12). Fig. 12 shows that the light output increases as the input power increases. The rate of increase decreases for higher input powers. This can be expected because of the poorer conversion efficiency at higher temperatures.

The normalized EL intensities at the chip surface along a certain line for the two different LED chips are compared with the normalized current densities and the normalized light output power intensities in the active layer as obtained from the numerical simulation for different input powers of 1 W, 2 W, 3 W, and 4 W, as shown in Fig. 13. The results show that the trend of the variation of the normalized current density and the normalized light output intensity with the position for the present numerical simulation. They are similar to that with the normalized EL intensity from the LED chip. In both the experimental and numerical simulation results, the increment decreases gradually when the input power increases. This phenomenon may be a result of the lower conversion efficiency due to thermal effects. The results of the normalized light output power intensity of the numerical computation have already extracted the heat loss from the nonradiative recombination since the conversion efficiency is taken into account in our model. Therefore, the magnitude of the normalized light output power intensities is closer to that of the normalized EL intensities in comparison with the normalized current density case.

A numerical simulation of the multimicrochip LED operated under a full-wave condition was performed. The apparent power is usually employed for the multimicrochip LED under the full-wave operation. For the alternating current condition, the apparent power is computed by multiplying the root-mean-square current (I_{rms}) by the root-mean-square voltage (V_{rms}). When the impedance is a pure resistance, the apparent power is the same as the true power. The LED is driven when the voltage is over the threshold. Under the threshold voltage, the forward current is not functional. Therefore, the true power is less than the value of apparent power. Fig. 14 shows the simulated instant average junction temperature under an apparent power of 6 W for full-wave operation after the quasi-steady state has been reached. The range of oscillation of the junction temperature between the maximum and minimum values is about 30 K. The time average junction temperature under this apparent power is about 400 K, which is lower than the junction temperature for the same multimicrochip LED under the same input power under dc operation (410.9 K). However, the instant maximum junction temperature under the full-wave operation (about 415 K) is still higher than the junction temperature under dc operation.

In this paper, the experiments do not go beyond a 4-W input power since the junction temperature at this point is near 380 K. However, a numerical simulation is still carried out to investigate the saturation effect under higher input powers. Fig. 15 shows the difference between the maximum junction temperature and minimum junction temperature in the active layer of both LED chips under

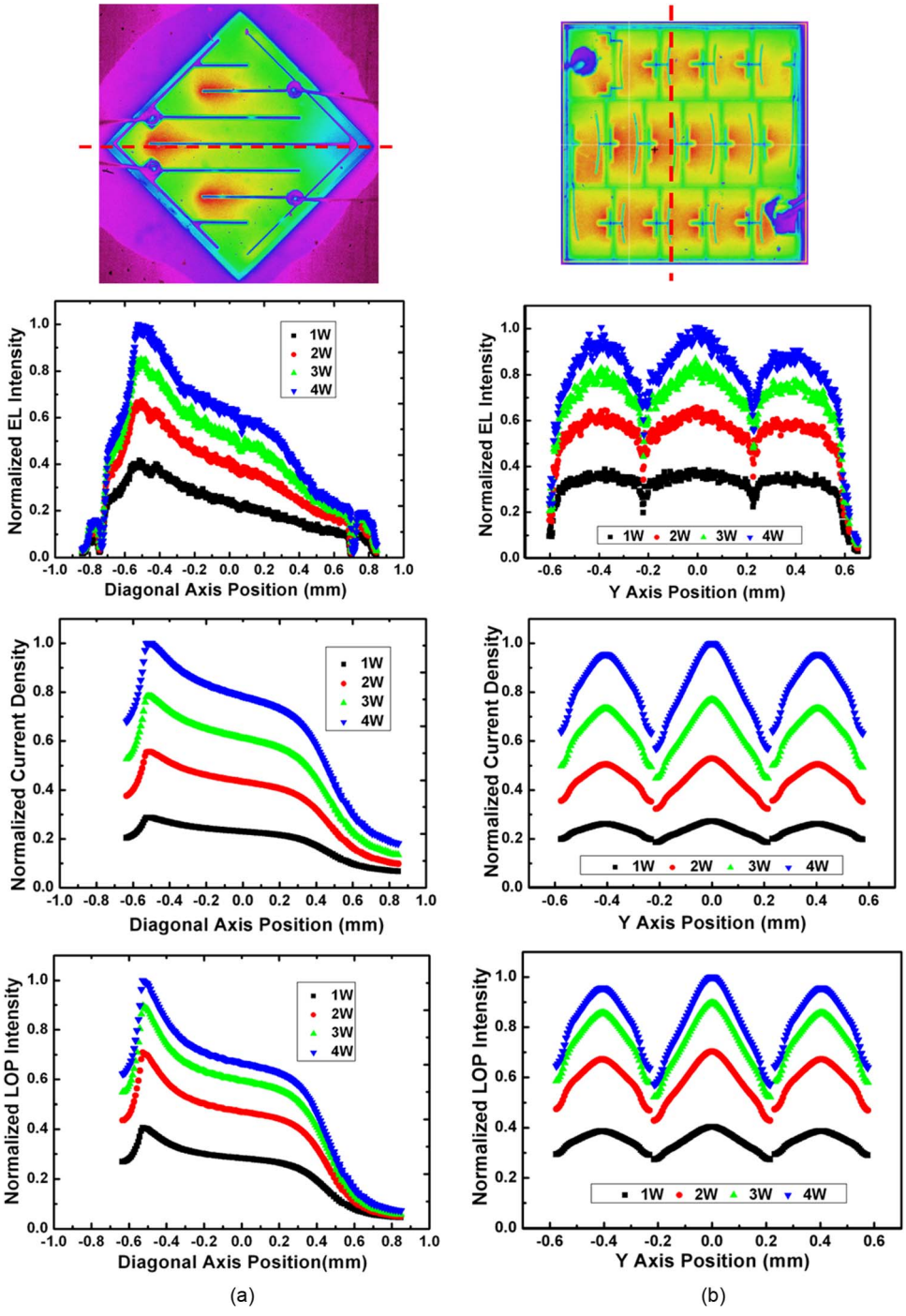

Fig. 13. Normalized EL intensities (measured) and the normalized current density (simulated) and light output power (LOP) intensities (simulated) under different input power for the two different types of LED chip. (a) Single chip LED with interdigitated mesa geometry. (b) Multimicrochip LED.

different operating conditions. The time average junction temperature is used for the multimicrochip LED under full-wave operation. The temperature difference in the multimicrochip LED under full-wave operation is about 10 K at an apparent power of 8 W, while that in the single-chip LED under dc operation is about 27 K. It is due to the value of apparent power (8 W) higher than the true power under full-wave operation. Otherwise, the current crowding problem is more serious in the

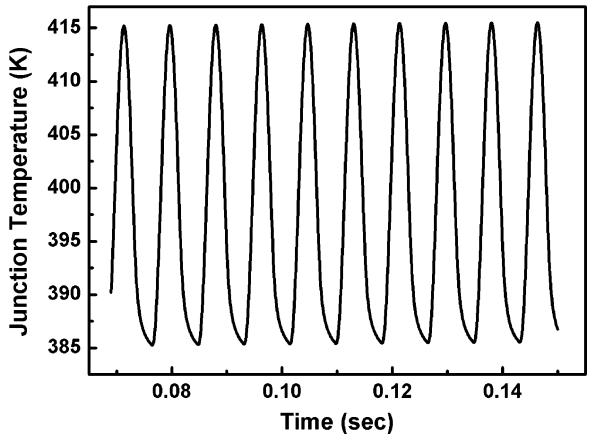

Fig. 14. Variation of the simulated average junction temperature with time for the multimicrochip LED under the full-wave operation with an apparent power 6 W during the quasi-steady state stage.

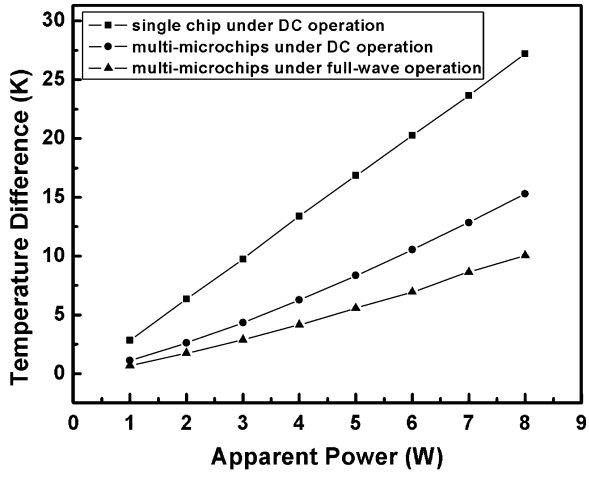

Fig. 15. Simulated temperature difference between the maximum and minimum junction temperature at the active layer of the LED chips for different apparent powers.

single-chip LED under dc operation. The temperature difference for the multimicrochip LED under the full-wave operation is the smallest. A higher temperature difference on a LED chip will induce more serious thermal stress effects and reduce the lifetime of the LED chip. Therefore, in terms of the time averaged junction temperature, the junction temperature of the multimicrochip LED under full-wave operation will not only be lower, but the temperature difference in the active layer will also be lower under the same input power operation. The difference in the instant maximum and minimum junction temperatures is 30 K at an apparent power of 6 W, but this is still higher than the temperature difference in the active layer of the single-chip LED (20.3K). The lifetime of the multi-microchip LED under full-wave operation may be reduced due to the nonuniformity of the temperature difference in this time frame.

The light output power is calculated for different input (apparent) powers under dc and full-wave operation, as shown in Fig. 16. The light output power first increases quickly and then more slowly as the input power increases. Due to the poorer conversion efficiency, the light output power of the single-chip LED becomes saturated when the input power exceeds 6 W. When the light output power reaches the saturation stage, the increase in energy due to increasing the input power mainly contributes to heating the LED chip leading to thermal failure of the LED chip. From Fig. 16, we can

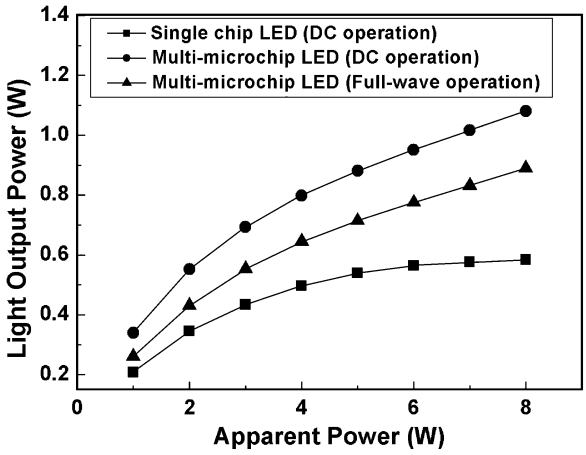

Fig. 16. Numerical simulation results of the light output power for two LED chips at different apparent powers under different operating conditions.

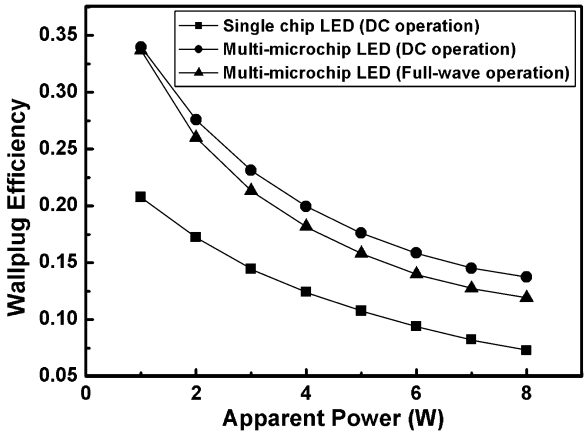

Fig. 17. Calculated wall plug efficiency of the two LED chips at different apparent powers under different operating conditions.

see that the light output power of the multimicrochip LED whether driven by dc or full-wave operation does not reach the saturation stage for the input power considered here. Since the value of apparent power of the multimicrochip LED under full-wave operation is higher than the true power, the light output power of the multimicrochip LED driven under full-wave operation is lower than for the dc driven one. The true power is calculated for different apparent powers. The wall plug efficiency is defined as the ratio of the light output power to true power. It is shown in Fig. 17. When the input power is higher, the wall plug efficiency decreases. The single-chip LED has a lower wall plug efficiency than the multimicrochip LED. The wall plug efficiency of the multimicrochip LED driven by full-wave operation is almost the same as that driven by dc power at an input power of 1 W. The true power is lower than the apparent power under the full-wave operation. When the input power is larger, the wall plug efficiency of the multimicrochip LED driven under full-wave operation becomes smaller than that driven by the dc power and the difference becomes large.

4. Conclusion

In this paper, a 3-D numerical model taking into account the coupling effect of the thermal and electrical characteristics has been developed to investigate two types of lateral-injection GaN-based LED chip with multimicrochip and single-chip configurations with interdigitated mesa

geometry. Moreover, the junction temperature, EL intensity, and light output power have been measured under dc operation. There is a good agreement between the light output power intensity distribution obtained from the present numerical simulations with consideration of the thermal effect and the EL intensity distribution from the experimental measurements. A numerical simulation has been also carried out for the multimicrochip LED under full-wave operation. In terms of thermal performance, the calculated junction temperature of the multimicrochip LED under dc operation is the most uniform. The junction temperature and the nonuniformity of the temperature in the LED chip increases as the input power increases. The multimicrochip LED under dc operation also has the highest light output power and best wall plug efficiency. Therefore, it has the best light output performance. For the single-chip LED with the interdigitated mesa geometry, the light output power has been saturated at lower input powers. On the other hand, when the input power increases, the light output power of the multimicrochip LED under both dc and full-wave operation increases continuously for the input power considered in this paper.

References

[1] S. H. Tu, J. C. Chen, F. S. Hwu, G. J. Sheu, F. L. Lin, S. Y. Kuo, J. Y. Chang, and C. C. Lee, "Characteristics of current distribution by designed electrode patterns for high power ThinGaN LED," *Solid State Electron.*, vol. 54, no. 11, pp. 1438–1443, Nov. 2010.

[2] Y. C. Hsu, Y. K. Lin, M. H. Chen, C. C. Tsai, J. H. Kuang, S. B. Huang, H. L. Hu, Y. I. Su, and W. H. Cheng, "Failure mechanisms associated with lens shape of high-power LED modules in aging test," *IEEE Trans. Electron Devices*, vol. 55, no. 2, pp. 689–694, Feb. 2008.

[3] C. K. Li and Y. R. Wu, "Study on the current spreading effect and light extraction enhancement of vertical GaN/InGaN LEDs," *IEEE Trans. Electron Devices*, vol. 59, no. 2, pp. 400–407, Feb. 2012.

[4] P. Wang, W. Wei, B. Cao, Z. Gan, and S. Liu, "Simulation of current spreading for GaN-based light-emitting diodes," *Opt. Laser Technol.*, vol. 42, no. 5, pp. 737–740, Jul. 2010.

[5] H. Kim, K. K. Kim, K. K. Choi, H. Kim, J. O. Song, J. Cho, K. H. Baik, C. Sone, Y. Park, and T. Y. Seong, "Design of high-efficiency GaN-based light-emitting diodes with vertical injection geometry," *Appl. Phys. Lett.*, vol. 91, no. 2, pp. 023510-1–023510-3, Jul. 2007.

[6] G. J. Sheu, F. S. Hwu, J. C. Chen, J. K. Sheu, and W. C. Lai, "Effect of the electrode pattern on current spreading and driving voltage in a GaN/sapphire LED chip," *J. Electrochem. Soc.*, vol. 155, no. 10, pp. H836–H840, 2008.

[7] A. Chakraborty, L. Shen, H. Masui, S. P. DenBaars, and U. K. Mishra, "Interdigitated multipixel arrays for the fabrication of high-power light-emitting diodes with very low series resistances," *Appl. Phys. Lett.*, vol. 88, no. 18, pp. 181120-1–181120-3, May 2006.

[8] J. P. Ao, "Monolithic integration of GaN-based LEDs," *J. Phys., Conf. Ser.*, vol. 276, no. 1, pp. 012001-1–012001-4, 2011.

[9] Z. Y. Fan, J. Y. Lin, and H. X. Jiang, "III-Nitride micro-emitter arrays: Development and applications," *J. Phys. D, Appl. Phys.*, vol. 41, no. 9, pp. 094001-1–094001-12, May 2008.

[10] J. T. Chu, C. C. Kao, H. W. Huang, W. D. Liang, C. F. Chu, T. C. Lu, H. C. Kuo, and S. C. Wang, "Effects of different n-electrode patterns on optical characteristics of large-area p-side-down InGaN light-emitting diodes fabricated by laser lift-off," *Jpn. J. Appl. Phys.*, vol. 44, no. 11, pp. 7910–7912, Nov. 2005.

[11] S. J. Wang, K. M. Uang, S. L. Chen, Y. C. Yang, S. C. Chang, T. M. Chen, C. H. Chen, and B. W. Liou, "Use of patterned laser liftoff process and electroplating nickel layer for the fabrication of vertical-structured GaN-based light-emitting diodes," *Appl. Phys. Lett.*, vol. 87, no. 1, pp. 011111-1–011111-3, Jul. 2005.

[12] D. W. Kim, H. Y. Lee, G. Y. Yeom, and Y. J. Sung, "A study of transparent contact to vertical GaN-based light-emitting diodes," *J. Appl. Phys.*, vol. 98, no. 5, pp. 053102-1–053102-4, Sep. 2005.

[13] M. R. Krames, O. B. Shchekin, R. Mueller-Mach, G. O. Mueller, L. Zhou, G. Harbers, and M. G. Craford, "Status and future of high-power light-emitting diodes for solid-state lighting," *J. Display Technol.*, vol. 3, no. 2, pp. 160–175, Jun. 2007.

[14] H. P. Zhao, G. Y. Liu, R. A. Arif, and N. Tansu, "Current injection efficiency quenching leading to efficiency droop in InGaN quantum well light-emitting diodes," *Solid State Electron.*, vol. 54, no. 10, pp. 1119–1124, Oct. 2010.

[15] I. E. Titkov, D. A. Sannikov, Y. M. Park, and J. K. Son, "Blue light emitting diode internal and injection efficiency," *AIP Adv.*, vol. 2, no. 3, pp. 032117-1–032117-4, Sep. 2012.

[16] R. M. Farrell, E. C. Young, F. Wu, S. P. DenBaars, and J. S. Speck, "Materials and growth issues for high-performance nonpolar and semipolar light-emitting devices," *Semicond. Sci. Technol.*, vol. 27, no. 2, p. 024001, Feb. 2012.

[17] H. Zhao, G. Liu, J. Zhang, J. D. Poplawsky, V. Dierolf, and N. Tansu, "Approaches for high internal quantum efficiency green InGaN light-emitting diodes with large overlap quantum wells," *Opt. Exp.*, vol. 19, no. S4, pp. A991–A1007, Jul. 2011.

[18] J. Zhang and N. Tansu, "Improvement in spontaneous emission rates for InGaN quantum wells on ternary InGaN substrate for light-emitting diodes," *J. Appl. Phys.*, vol. 110, no. 11, pp. 113110-1–113110-5, Dec. 2011.

[19] Y. K. Ee, J. M. Biser, W. Cao, H. M. Chan, R. P. Vinci, and N. Tansu, "Metalorganic vapor phase epitaxy of III-Nitride light-emitting diodes on nanopatterned AGOG sapphire substrate by abbreviated growth mode," *IEEE J. Sel. Topics Quantum Electron.*, vol. 15, no. 4, pp. 1066–1072, Jul./Aug. 2009.

[20] Y. K. Ee, X.-H. Li, J. Biser, W. Cao, H. M. Chan, R. P. Vinci, and N. Tansu, "Abbreviated MOVPE nucleation of III-nitride light-emitting diodes on nano-patterned sapphire," *J. Crystal Growth*, vol. 312, no. 8, pp. 1311–1315, Apr. 2010.
[21] Y. Li, S. You, M. Zhu, L. Zhao, W. Hou, T. Detchprohm, Y. Taniguchi, N. Tamura, S. Tanaka, and C. Wetzel, "Defect-reduced green GaInN/GaN light-emitting diode on nanopatterned sapphire," *Appl. Phys. Lett.*, vol. 98, no. 15, pp. 151102-1–151102-3, Apr. 2011.
[22] X. H. Li, S. R. Song, Y. K. Ee, P. Kumnorka ew, J. F. Gilchrist, and N. Tansu, "Light extraction efficiency and radiation patterns of III-Nitride light-emitting diodes with colloidal microlens arrays with various aspect ratios," *IEEE Photon. J.*, vol. 3, no. 3, pp. 489–499, Jun. 2011.
[23] Y. K. Ee, P. Kumnorkaew, R. A. Arif, H. Tong, J. F. Gilchrist, and N. Tansu, "Light extraction efficiency enhancement of InGaN quantum wells light-emitting diodes with polydimethylsiloxane concave microstructures," *Opt. Exp.*, vol. 17, no. 16, pp. 13 747–13 757, Aug. 2009.
[24] E. Rangel, E. Matioli, Y. S. Choi, C. Weisbuch, J. S. Speck, and E. L. Hu, "Directionality control through selective excitation of low-order guided modes in thin-film InGaN photonic crystal light-emitting diodes," *Appl. Phys. Lett.*, vol. 98, no. 8, pp. 081104-1–081104-3, Feb. 2011.
[25] A. Sztein, H. Ohta, J. Sonoda, A. Ramu, J. E. Bowers, S. P. DenBaars, and S. Nakamura, "GaN-based integrated lateral thermoelectric device for micro-power generation," *Appl. Phys. Exp.*, vol. 2, no. 11, pp. 111003-1–111003-3, Nov. 2009.
[26] H. Tong, J. Zhang, G. Liu, J. A. Herbsommer, G. S. Huang, and N. Tansu, "Thermoelectric properties of lattice-matched AlInN alloy grown by metal organic chemical vapor deposition," *Appl. Phys. Lett.*, vol. 97, no. 11, pp. 112105-1–112105-3, Sep. 2010.
[27] J. Zhang, H. Tong, G. Liu, J. A. Herbsommer, G. S. Huang, and N. Tansu, "Characterizations of Seebeck coefficients and thermoelectric figures of merit for AlInN alloys with various In-contents," *J. Appl. Phys.*, vol. 109, no. 5, pp. 053706-1–053706-6, Mar. 2011.
[28] H. Kim, J. Cho, J. W. Lee, S. Yoon, H. Kim, C. Sone, Y. Park, and T. Y. Seong, "Consideration of the actual current-spreading length of GaN-based light-emitting diodes for high-efficiency design," *IEEE J. Quantum Electron.*, vol. 43, no. 8, pp. 625–632, Aug. 2007.
[29] H. Kim, J. M. Lee, C. Huh, S. W. Kim, D. J. Kim, S. J. Park, and H. Hwang, "Modeling of a GaN-based light-emitting diode for uniform current spreading," *Appl. Phys. Lett.*, vol. 77, no. 12, pp. 1903–1904, Sep. 2000.
[30] H. Kim, S. J. Park, H. Hwang, and N. M. Park, "Lateral current transport path, a model for GaN-based light-emitting diodes: Applications to practical device designs," *Appl. Phys. Lett.*, vol. 81, no. 7, pp. 1326–1328, Aug. 2002.
[31] X. Guo and E. F. Schubert, "Current crowding in GaNInGaN light emitting diodes on insulating substrates," *J. Appl. Phys.*, vol. 90, no. 8, pp. 4191–4195, Oct. 2001.
[32] S. Hwang and J. Shim, "A method for current spreading analysis and electrode pattern design in light-emitting diodes," *IEEE Trans. Electron Devices*, vol. 55, no. 5, pp. 1123–1128, May 2008.
[33] J. C. Chen, G. J. Sheu, F. S. Hwu, H. I. Chen, J. K. Sheu, T. X. Lee, and C. C. Sun, "Electrical-optical analysis of a GaN/Sapphire LED chip by considering the resistivity of the current-spreading layer," *Opt. Rev.*, vol. 16, no. 2, pp. 213–215, Mar. 2009.
[34] N. Narendran, Y. Gu, J. P. Freyssinier, H. Yu, and L. Deng, "Solid-state lighting: Failure analysis of white LEDs," *J. Crystal Growth*, vol. 268, no. 3/4, pp. 449–456, Aug. 2004.
[35] S. Chhajed, Y. Xi, Y. L. Li, T. Gessmann, and E. F. Schubert, "Influence of junction temperature on chromaticity and color-rendering properties of trichromatic white-light sources based on light-emitting diodes," *J. Appl. Phys.*, vol. 97, no. 5, pp. 054506-1–054506-8, Mar. 2005.
[36] E. F. Schubert, *Light-Emitting Diodes*, 2nd ed. Cambridge, U.K.: Cambridge Univ. Press, 2006.
[37] J. Kettle, R. M. Perks, and P. Dunstan, "Localised joule heating in AlGaInP light emitting diodes," *Electron. Lett.*, vol. 42, no. 19, pp. 1122–1123, Sep. 2006.
[38] F. S. Hwu, J. Sheu, M. T. Lin, and J. C. Chen, "Method for determining the junction temperature current light-emitting diodes," *IET Sci. Meas. Technol.*, vol. 3, no. 2, pp. 159–164, Mar. 2009.
[39] F. S. Hwu, C. H. Yang, and J. C. Chen, "Method for measuring the mean junction temperature of alternating current light-emitting diodes," *Meas. Sci. Technol.*, vol. 22, no. 4, pp. 045701-1–045701-6, Apr. 2011.
[40] M. V. Bogdanov, K. A. Bulashevich, I. Y. Evstratov, A. I. Zhmakin, and S. Y. Karpov, "Coupled modeling of current spreading, thermal effects and light extraction in III-nitride light-emitting diodes," *Semicond. Sci. Technol.*, vol. 23, no. 12, pp. 125023-1–125023-10, Dec. 2008.
[41] M. V. Bogdanov, K. A. Bulashevich, I. Y. Evstratov, and S. Y. Karpov, "Current spreading, heat transfer, and light extraction in multi-pixel LED array," *Phys. Stat. Sol. (C)*, vol. 5, no. 6, pp. 2070–2072, May 2008.
[42] F. S. Hwu, J. C. Chen, S. H. Tu, G. J. Sheu, H. I. Chen, and J. K. Sheu, "A numerical study of thermal and electrical effects in a vertical LED Chip," *J. Electrochem. Soc.*, vol. 157, no. 1, pp. H31–H37, 2010.
[43] H. H. Yen, W. Y. Yeh, and H. C. Kuo, "GaN alternating current light-emitting device," *Phys. Stat. Sol. (A)*, vol. 204, no. 6, pp. 2077–2081, Jun. 2007.
[44] W. W. Yeh, H. H. Yen, and Y. J. Chan, "The development of monolithic alternating current light-emitting diode," in *Proc. SPIE*, 2010, vol. 7939, pp. 793910-1–793910-4.
[45] J. Ibbetson and S. Heikman, "High voltage low current surface-emitting LED," U.S. Patent 7 985 970, Jul. 26, 2011.
[46] Y. J. Lee, C. J. Lee, and C. H. Chen, "Estimating the junction temperature of InGaN and AlGaInP light-emitting diodes," *Jpn. J. Appl. Phys.*, vol. 50, no. 4, pp. 04DG18-1–04DG18-5, Apr. 2011.
[47] G. E. Myers, *Analytical Methods in Conduction Heat Transfer*, 2nd ed. Madison, WI, USA: AMCHT, 1998, Appendix A.
[48] J. P. Holman, *Heat Transfer*, 9th ed. Singapore: McGraw-Hill, 2010, Appendix A.